ARCHIVES OF METALLURGY
Volume 48 2003 Issue 2

ANDRZEJ BACZMAŃSKI *, STANISŁAW SKRZYPEK**, CHEDLI BRAHAM***,
WILFRID SEILER***, KRZYSZTOF WIERZBANOWSKI*

SELF-CONSISTENT DIFFRACTION ELASTIC CONSTANTS IN RESIDUAL STRESS MEASUREMENT WITH GRAZING INCIDENT ANGLE GEOMETRY

SAMOUZGODNIONE STAŁE ELASTYCZNE W POMIARACH NAPRĘŻEŃ WEWNĘTRZNYCH METODĄ STAŁEGO KĄTA PADANIA

The method based on the grazing incident angle geometry was applied for stress measurement in surface layers of polycrystalline samples. The advantage of this geometry is a constant penetration depth of the *X*-ray beam during experiment, however, the interpretation of experimental data is more difficult than for the standard technique. Diffraction elastic constants have to be calculated for various *hkl* reflections. The influence of elastic anisotropy on the results of stress measurement is studied.

Metoda oparta na geometrii stałego kąta padania zastosowana została do pomiaru naprężeń w warstwach powierzchniowych próbek polikrystalicznych. Zaletą metody jest stała głębokość wnikania promienia rentgenowskiego podczas pomiarów, jednak interpretacja danych doświadczanych jest trudniejsza niż w przypadku standardowej techniki. Dyfrakcyjne stałe elastyczne muszą być obliczone dla różnych refleksów *hkl*. Rozważony jest wpływ anizotropii elastycznej materiału na wyniki pomiaru naprężeń.

1. Introduction

The macro-stresses created due to thermal or mechanical treatment of polycrystalline material are usually heterogeneous and they change with the depth bellow sample surface. A significant stress gradient can be found, for example, in shot peened near surface volume [1] and in plasma sprayed [2] or vapour deposited coatings [3]. The diffraction $\sin^2\psi$ method of residual stress determination is based on the measurement of interplanar spacings

* WYDZIAŁ FIZYKI I TECHNIKI JĄDROWEJ, AKADEMIA GÓRNICZO-HUTNICZA, 30-059 KRAKÓW, AL. MICKIEWICZA 30
** WYDZIAŁ METALURGII I INŻYNIERII MATERIAŁOWEJ, AKADEMIA GÓRNICZO-HUTNICZA, 30-059 KRAKÓW, AL. MICKIEWICZA 30
*** LM3, CNRS ESA 8006, ECOLE NATIONALE SUPÉRIEURE D'ARTS ET MÉTIERS, 151, BD DE L'HOPITAL, 75013 PARIS, FRANCE

for one crystallographic plane $\{hkl\}$ at various orientations of the scattering vector, characterised by φ and ψ angles (Fig. 1) [4]. Consequently, the penetration depth of the X-ray radiation changes for different ψ angles [5].

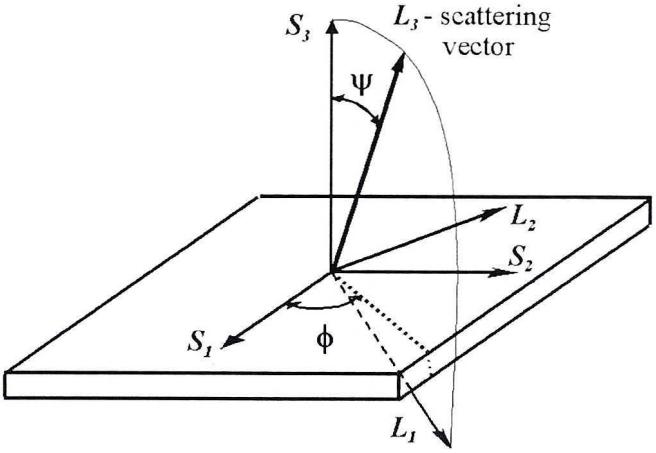

Fig. 1. Geometry of the $\sin^2\psi$ methods. The $<d(\psi, \phi)>_{\{hkl\}}$ spacings are measured along L_3 axis in **L**-system and the stresses σ^{L}_{ij} are defined with respect to the **S** – sample system

Recently, the geometry (named g–$\sin^2\psi$ method) based on the grazing incidence angle X-ray diffraction was applied for measurement of the interplanar spacings [6-10]. Using this method, the non-destructive analysis of the heterogeneous stresses for different (well defined) volumes bellow the sample surface can be done. Stresses can be measured at small depths of about 0.1-5 μm. The g–$\sin^2\psi$ method is characterised by low and constant incident angle (α in Fig. 2) and by different lengths and orientations of scattering vector. In contrast with the standard $\sin^2\psi$ methods, the measurements are performed for different sets of $\{hkl\}$ planes using appropriate values of $\theta_{\{hkl\}}$ scattering angles (Fig.2) [6-10].

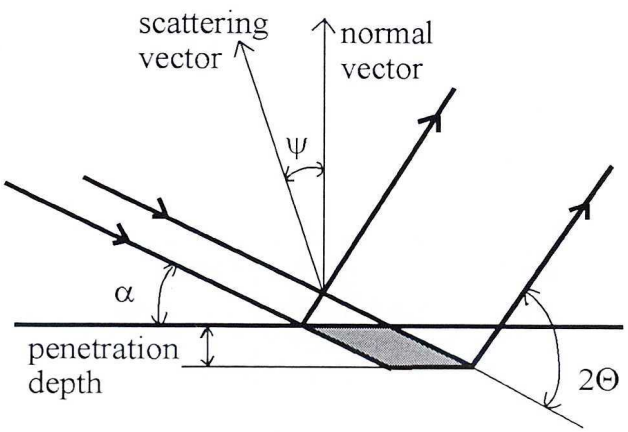

Fig. 2. Geometry used in the g–$\sin^2\psi$ method. The penetration depth (t in equation (3)) for low incident angle α (fixed during experiment) and orientation of scattering vector (characterised by ψ) are shown

The $g-\sin^2\psi$ method is based on the non-standard geometry and it requires a new interpretation of experimental data using properly calculated (or measured) diffraction elastic constants. Hence, the influence of elastic anisotropy on the interpretation of stress measurement is considered using various theoretical models.

2. Grazing incident X-ray diffraction

In diffraction methods the mean interplanar spacing $<d(\phi, \psi)>_{\{hkl\}}$ averaged only for *reflecting grains* which possess the scattering vector normal to the $\{hkl\}$ crystallographic planes is determined. For a quasi-isotropic sample (without texture), the mean interplanar spacing measured in the L_3 direction (Fig. 1) is given by the well known relation [4]:

$$<d(\phi, \psi)>_{\{hkl\}} = \Big[s_1(hkl)(\sigma^I_{11} + \sigma^I_{22} + \sigma^I_{33}) + \frac{1}{2} s_2(hkl)(\sigma^I_{11}\cos^2\phi + \sigma^I_{22}\sin^2\phi + \sigma^I_{12}\sin 2\phi)$$
$$\sin^2\psi + \frac{1}{2} s_2(hkl)\sigma^I_{33}\cos^2\psi + \frac{1}{2} s_2(hkl)(\sigma^I_{13}\cos\phi + \sigma^I_{23}\sin\phi) \qquad (1)$$
$$\sin 2\psi \Big] d^\circ_{\{hkl\}} + d^\circ_{\{hkl\}}.$$

where: macro-stresses σ^I_{ij} are defined with respect to the *S*-system (Fig. 1), while $s_1(hkl)$ and $s_2(hkl)$ are the diffraction elastic constants for a quasi-isotropic sample.

Using the standard *X*-ray diffraction method the interplanar spacings are measured as a function of $\sin^2\psi$ for constant *hkl* reflection and ϕ angle, as well. In this case, the above equation expresses a linear character of $< d(\phi, \psi>_{\{hkl\}}$ vs. $\sin^2\psi$ graph for a biaxial stress state (i.e., for $\sigma^I_{33} = \sigma^I_{23} = \sigma^I_{13} = 0$) or it shows a splitting phenomenon if non-zero shear stresses σ^I_{23} and σ^I_{13} are present in the sample. The splitting, i.e., opposite curvature of the $<d(\phi, \psi)>_{\{hkl\}}$ vs. $\sin^2\psi$ plots can be observed when the measurements are performed for the ϕ and $\phi + \pi$ angles, respectively. For one phase material, due to low penetration depth of *X*-ray radiation the force perpendicular to the sample surface is not present in the analyzed volume and consequently σ^I_{33} is assumed to be equal to zero. In the standard $\sin^2\psi$ method a linear or elliptical regression is used to determine the stresses from $<d(\phi, \psi)>_{\{hkl\}}$ vs. $\sin^2\psi$ graphs for given *hkl* and ϕ parameters [4].

For textured samples the diffraction elastic constants depend on the orientation distribution function [11] and vary with ϕ and ψ angles. Consequently, the plots of $<\varepsilon'(\phi, \psi)>_{\{hkl\}}$ vs. $\sin^2\psi$ or of F_{11} vs. $\sin^2\psi$ are no more linear or elliptical. The measured interplanar spacings must be expressed by macro-stresses σ^I_{ij} using more general equation [12,13]:

$$<d(\phi, \psi)>_{\{hkl\}} = [F_{ij}(hkl, \psi, \phi)\,\sigma^I_{ij}]\,d^0 + d^0, \qquad (2)$$

where: $F_{ij}(hkl, \psi, \phi)$ are diffraction elastic constants for the *hkl* reflection.

Using the least square method for Eq.2, the fitting parameters (i.e., σ_{ij}^{I} and d^{0}) can be determined.

The non-standard $g-\sin^2\psi$ method is based on the grazing incident angle geometry in which a small incident angle (α in Fig. 2) is constant during measurements for various orientations of the scattering vector [8-10]. Hence, unlike in the standard $\sin^2\psi$ methods, the measurements must be performed for different sets of $\{hkl\}$ planes using various values of $\theta_{\{hkl\}}$ scattering angles (Fig. 2). In the standard measurements the orientation of scattering vector is given by two variable angles ϕ and ψ (Fig. 1), which can be changed independently. In the $g-\sin^2\psi$ geometry, only ϕ angle can be chosen arbitrarily, while ψ angle depends on the hkl reflection and a constant incident angle α (Fig. 2), i.e.: $\psi_{\{hkl\}} = \theta_{\{hkl\}} - \alpha$ [6-10]. Possible values of $\psi_{\{hkl\}}$ angles are limited to the number of hkl reflections measured in the experiment [9-10].

Using the $g-\sin^2\psi$ method, the measurement is performed for a near-surface volume, which is limited by absorption of the X-ray radiation. To define this volume, the path of the X-ray beam through the sample should be considered and the effective depth of penetration (t) can be defined [8-10].

$$t = \frac{1}{\mu\left[\frac{1}{\sin\alpha} + \frac{1}{\sin(2\theta - \alpha)}\right]}, \tag{3}$$

where: t is defined as the depth for which $(1-1/e)$ part of incident beam intensity is absorbed in the material, μ is the linear coefficient of absorption, α and θ are incident and scattering angles, respectively (Fig. 2).

The $g-\sin^2\psi$ method is based on the non-conventional geometry for which interplanar spacings $<d(\phi,\psi)>_{\{hkl\}}$ are measured for different hkl reflections [8-10]. Hence, for calculation of the macro-stress tensor the $<d(\phi,\psi)>_{\{hkl\}}$ spacings have to be transformed to the equivalent values of lattice parameter, i.e.: $<a(\phi,\psi>_{\{hkl\}} = <d(\phi,\psi)>_{\{hkl\}}\sqrt{h^2 + k^2 + l^2}$ for cubic structure.

Consequently, the macro-stresses can be determined using the least square fitting procedure for a general equation:

$$<a(\psi,\phi)>_{\{hkl\}} = [F_{ij}(hkl,\psi,\phi)\sigma_{ij}^{I}]\, a^{0} + a^{0} \tag{4}$$

where only a single value of a_0 parameter for a stress free material, instead of different values of $d_{\{hkl\}}^{0}$ spacings, is used (cf. Eq. 2).

3. Calculation of diffraction elastic constants

Let us consider polycrystalline material under applied load for which the diffraction elastic constants are defined as [12,13]:

$$<\varepsilon'(\psi\psi,\varphi>_{\{hkl\}} = <\varepsilon'_{33}>_{\{hkl\}} = R'_{ij}(hkl,\phi,\psi,f(g))\sigma^{I}_{ij}, \quad (5)$$

where: $<\varepsilon'(\phi,\psi)>_{\{hkl\}}$ or $<\varepsilon'_{33}>_{\{hkl\}}$ is the strain in L_3 direction averaged over the volume of reflecting grains, R'_{ij} are the diffraction elastic constants defined with respect to the $\boldsymbol{L}$ coordinate system (Fig. 1), $f(g)$ is the orientation distribution function characterizing crystallographic texture [11] and σ^{I}_{ij} are the applied or residual macro-stresses expressed in the $\boldsymbol{L}$ system (Fig.1).

An alternative formula for diffraction elastic constants may be proposed when the applied stress (σ^{I}_{ij}) is defined in the $\boldsymbol{S}$ system (Fig. 1) and so obtained coefficients are denoted by F_{ij} [12,13]:

$$<\varepsilon'(\psi,\phi)>_{\{hkl\}} = <\varepsilon'_{33}> = F_{ij}(hkl,\psi,\phi,f(g))\sigma^{I}_{ij} \quad (6)$$

The F_{ij} coefficients are not tensor components because they relate the stresses σ^{I}_{ij} expressed in $\boldsymbol{S}$ system to the strain $<\varepsilon'_{33}>_{\{hkl\}}$ defined along L_3 axes of $\boldsymbol{L}$-frame. Using the appropriate transformation, the F_{ij} diffraction elastic constants can be calculated from the R_{ij} ones, i.e.:

$$F_{ij}(hkl,\phi,\psi,f(g)) = R'_{mn}(hkl,\phi,\psi,f(g))\gamma_{mi}\,\gamma_{nj}, \quad (7)$$

where the γ matrix transforms stresses from the $\boldsymbol{S}$ to $\boldsymbol{L}$-system, i.e.: $\sigma^{I}{}'_{mn} = \gamma_{mi}\,\gamma_{nj}\,\sigma^{I}_{ij}$. It should be emphasised that the R'_{ij} constants, in equations (5) and (7), depend on the orientation of the $\boldsymbol{L}$ system with respect to the $\boldsymbol{S}$ system if the sample is textured. However, in the case of polycrystal with random grain orientations (so called quasi-isotropic sample), the R'_{ij} constants do not vary with ϕ and ψ angles because the sample is isotropic [12,13].

The simplest models, i.e., V o i g t [14] and R e u s s [15] methods for R'_{ij} calculation are based on the hypothesis of homogeneity of strain or stress, respectively. These models define the upper and lower limits of the diffraction elastic constants, which can be determined for the polycrystalline material. In more realistic models the interaction between grains is taken into account in R'_{ij} calculations. For example in the K r ö n e r [16] method, used in this work, the grain is approximated by an ellipsoidal inclusion, which is embedded into homogenous matrix. The elastic properties of the matrix are defined as the average one for all grains and they can be determined using the self-consistent scheme [17,18].

a) R e u s s model

In this approach the local stress σ_{ij} is assumed to be uniform across the sample for all polycrystalline grains, i.e., $\sigma_{ij} = \sigma^{I}_{ij}$ [15]. The local strain in the L_3 direction (Fig.1) is equal to:

$$\varepsilon'_{33} = s'_{33ij}\,\sigma'_{ij} = s'_{33ij}\,\sigma^{I}{}'_{ij} \qquad \text{and} \qquad <\varepsilon'_{33}>_{\{hkl\}} = <s'_{33ij}>_{\{hkl\}}\,\sigma^{I}{}'_{ij} \quad (8)$$

where s'_{ijkl} is the compliance tensor for a single crystal. Consequently, using the R e u s s model, diffraction elastic constants can be expressed through [13]:

$$R^{R}_{ij} = < s'_{33ij} >_{\{hkl\}} = \frac{\int_0^{2\pi} s'_{33ij}(g) f(g) d\zeta}{\int_0^{2\pi} f(g) d\zeta}, \tag{9}$$

where integration is carried over all g orientations representing *the reflecting grains* and ζ is the rotation angle of the crystallite around scattering vector (being perpendicular to the $\{hkl\}$ planes).

b) V o i g t model

The uniform local strain (ε_{ij}) is assumed to be equal to the macro-strain value (ε^{I}_{ij}), i.e., $\varepsilon_{ij} = \varepsilon^{I}_{ij}$ in the V o i g t model [14]. Local stress is expressed through $\sigma'_{ij} = c'_{ijkl}\varepsilon'_{kl}$, where c'_{ijkl} is the single crystal stiffness tensor defined with respect to the ***L***-frame. The average stress, marked *[...]*, is calculated over the whole sample volume, i.e.:

$$\sigma^{I\prime}_{ij} = [c'_{ijkl}\,\varepsilon'_{kl}] = [c'_{ijkl}]\,\varepsilon^{I\prime}_{kl}. \tag{10}$$

$$<\varepsilon'_{33}>_{\{hkl\}} = \varepsilon^{I}{}_{33}' = [c']^{-1}_{33ij}\,\sigma^{I}_{ij}.$$

Finally, the R^{V}_{ij} constants are equal to [13]:

$$R^{V}_{ij} = [c']^{-1}_{33ij}. \tag{11}$$

The texture function $f(g)$ is used in calculation of the R^{V}_{ij} constants. In this model *all grains* from the irradiated volume contribute to the average:

$$[c'_{ijkl}] = \frac{1}{8\pi^2}\int_E c'_{ijkl}(g) f(g) dg. \tag{12}$$

In the above equation the single crystal stiffness $c'_{ijkl}(g)$ (considered in the ***L***-system) are integrated over the whole orientation space E.

c) Kröner approach calculated using self-consistent model

In the self-consistent model the polycrystalline grain is considered as an ellipsoidal inclusion inside the homogeneous matrix [17,18]. The existence of the A'_{mnkl} concentration tensor relating the local strain (e.g., grain strain) ε'_{mn} to the macro-strain $\varepsilon^{I}_{kl}{}'$ is postulated:

$$\varepsilon'_{mn} = A'_{mnkl}\,\varepsilon^{I\prime}_{kl}. \tag{13}$$

Substituting the H o o k ' s law for macro-tensors ($\varepsilon^{I\prime}_{ij} = S'_{ijkl}\,\sigma^{I\prime}_{kl}$, where S'_{ijkl} is the sample compliance tensor expressed in the ***L***-system) in the above equation, a grain strain can be related to the macro-stress, i.e.:

$$\varepsilon'_{33} = X'_{33kl}\,\sigma^{I\prime}_{kl}, \tag{14}$$

where: $X'_{ijkl} = A'_{ijmn}\,S'_{mnkl}$.

Finally, the diffraction elastic constants R_{ij}^{K} are defined as:

$$R_{ij}^{K} = < X'_{33ij} >_{\{hkl\}} = \frac{\int_{0}^{2\pi} X'_{33ij}(g) f(g)\, d\zeta}{\int_{0}^{2\pi} f(g)\, d\zeta}, \tag{15}$$

where the integration is carried over all g orientations representing reflecting grains, similarly like in equation (9).

For calculation of the X'_{ijkl} tensor the macro-compliance tensor S'_{ijkl} for polycrystalline aggregate must be known. This tensor can be calculated using the self-consistent model [16-18] and assuming the ellipsoidal shape of inclusion (Eshelby approach [19]) representing polycrystalline grain. In the present work the theory proposed by B e r v e i l l e r and L i p i ń s k i was used for self-consistent calculations [17,18]. In this formalism, the local stresses can be expressed by the macro-stresses:

$$\sigma'_{ij} = c'_{ijnm}\, \varepsilon'_{mn} = c'_{ijmn}\, \{A'_{mnkl}\, \varepsilon^{I}_{kl}{}'\}, \tag{16}$$

where equation (13) was substituted into the H o o k ' s law defined for a grain.
Integrating both sides of the relation (16) over the whole sample volume (i.e., over all grain orientations and taking the texture function as the weighting one) the macrostress can be calculated:

$$\sigma^{I}_{ij}{}' = \{\int_{E} c'_{ijmn} A'_{mnkl} f(g)\, dg\}\, \varepsilon^{I}_{kl}{}'. \tag{17}$$

Comparing this equation with the H o o k ' s law for macro-tensors ($\sigma^{I}_{ij}{}' = C'_{ijnm}\, \varepsilon^{I}_{mn}{}'$), the formula for macro-compliance and macro-stiffness tensors (expressed in $\boldsymbol{L}$- system) can be found:

$$C'_{ijkl} = \int_{E} c'_{ijmn} A'_{mnkl}(g) f(g)\, dg \qquad \text{and} \qquad \boldsymbol{S}' = (\boldsymbol{C}')^{-1}. \tag{18}$$

The $\boldsymbol{S}$' tensor can be calculated only if the $\boldsymbol{A}$' tensor is known, and inversely. This is the reason why the self-consistent procedure must be applied for determination of both of them. Finally, knowing $\boldsymbol{A}$' and $\boldsymbol{S}$' tensors, the $\boldsymbol{X}$' tensor can be calculated (Eq. 14). The latter one is necessary for the calculation of diffraction elastic constants using Eq.15.

4. Experimental results and discussion

The interplanar spacings were measured using grazing incident geometry for two exemplary sets of samples, i.e., for the polycrystalline materials having low (TiN) and high

(ferrite and austenite) elastic anisotropy of crystallites. To show the influence of crystal anisotropy on diffraction elastic constants, the s_1 and s_2 quasi-isotropic constants were calculated for all studied materials. The single crystal elastic constants (listed in Table 1) and a constant orientation distribution function $f(g)=1$ were used for the presented models. As expected, a large variation of s_1 and s_2 for different hkl reflections was found for ferrite (Fig. 3) and austenite (not shown), while not significant changes of diffraction elastic constants were observed for the TiN polycrystal (Fig.3).

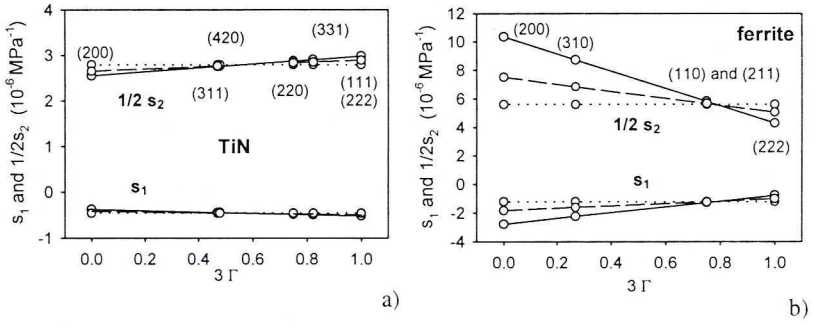

Fig. 3. The s_1 and $^1/_2\ s_2$ constants as a function of the anisotropy parameter $3\Gamma = 3\dfrac{(h^2k^2 + h^2l^2 + k^2l^2)}{(h^2 + k^2 + l^2)^2}$ calculated from the single crystal data (Table 1) using V o i g t (dotted line), K r ö n e r (dashed line) and R e u s s (solid line) models. The results for a) small crystal anisotropy (TiN), and b) large crystal anisotropy (ferrite), are shown

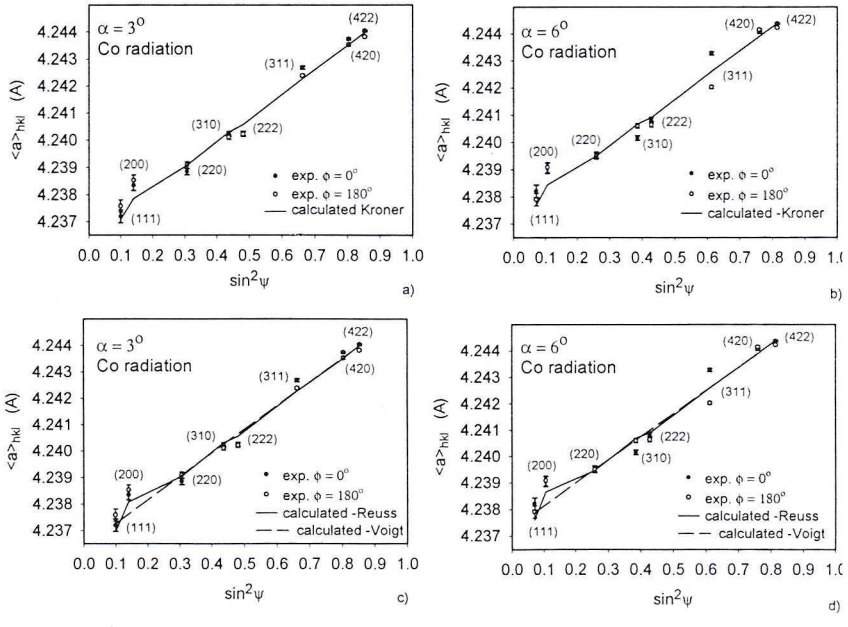

Fig. 4. The $\langle a(\phi,\psi)\rangle_{\{hkl\}}$ lattice parameters fitted to the experimental points for mechanically polished ferritic steel. The experimental points are compared with values obtained by fitting procedure using diffraction elastic constants calculated by K r ö n e r (*a,b*), R e u s s and V o i g t (*c,d*) methods. Theoretical points are connected by lines

a) TiN coating

TiN coating (thickness of 5 μm) was deposited on WC substrate using chemical vapour deposition process. The tensile biaxial stress state in the coating arises due to sample cooling from the high temperature (1173 K) of deposition process to the room temperature ($\Delta T \cong 900$ K). This stress is caused by the difference of thermal expansion coefficients for the TiN coating ($\alpha_T = 9.35 \times 10^{-6}$ K^{-1}) and WC substrate ($\alpha_T = 6 \times 10^{-6}$). For this sample the Co - Kα radiation was used to determine the $\langle a(\phi,\psi)\rangle_{\{hkl\}}$ vs. $sin^2\psi$ curves for $\phi = 0°$ and $\phi = 180°$ and for two different incident angles α (Fig.4 and Table 2).

b) Mechanically polished ferritic steel

The ferritic steel sample was examined by grazing incident method using the Cu - Kα radiation. The sample surface was mechanically polished. It should be stated that high absorption of Cu radiation in steel samples enables the measurements for extremely thin layer under the surface (0.1 - 1μm), in which the stress distribution cannot be determined by the standard techniques. The polished samples exhibit a very high quality of the surface (i.e., roughness $R_z \approx 0.1$ μm) and consequently the penetration depth of X-ray radiation can be defined even for Cu radiation. The $\langle a(\phi,\psi)\rangle_{\{hkl\}}$ vs. $sin^2\psi$ curves were determined for $\phi = 0°$ and $\phi = 90°$ and for three various incident angles α corresponding to different penetration depths t (Fig. 5 and Table 2).

c) Austenitic steel after grinding

The surface of austenitic steel was subjected to the grinding treatment in the S_1 direction (Fig. 1). In this case the asymmetry of planar stresses (i.e., $\sigma_{11} \neq \sigma_{22}$) and a large roughness of the surface is expected. Hence, the grazing incident method was applied using Cu and Fe radiations in order to study deeper volumes of the sample (over 1 μm). Again, the $\langle a(\phi,\psi)\rangle_{\{hkl\}}$ vs. $\sin^2\psi$ curves were determined for $\phi = 0°$ and $\phi = 90°$ and for three different incident angles α (Fig. 6 and Table 2).

To find the values of residual stresses, the experimental data were analysed using the least square fitting procedure and Eq. 4. The diffraction elastic constants (F_{ij}) were calculated from single crystal stiffness constants (Table 1) using the V o i g t, K r ö n e r and R e u s s models and assuming quasi-isotropic materials (i.e., $f(g) = 1$). Two principal components of stress tensor (i.e., σ_{11} and σ_{22} assuming $\sigma_{33} = 0$) were found for the steel samples. As expected, due to the symmetry of surface treatment, approximately equal values of both components (i.e., $\sigma_{11} = \sigma_{22}$) were found in the ferritic steel sample subjected to mechanical polishing (Table. 2). Different values of stresses were also measured for various penetration depths, i.e. the stress gradient was present in the near surface volume. Different values of principal stress components (i.e., $\sigma_{11} \neq \sigma_{22}$) were determined in the austenitic steel after grinding performed along the S_1 direction (Fig.1). Both components are positive and they depend on the penetration depth. In the case of TiN coating the equal principal stresses were expected ($\sigma_{11} = \sigma_{22}$) and the symmetry of coating deposition was verified by measurement of the $\langle a(\phi,\psi)\rangle_{\{hkl\}}$ vs. $sin^2\psi$ curves for $\phi = 0°$ and $\phi = 180°$. The tensile principal stress σ_{11} and a zero value of the shear stress σ_{33} were determined from the $\langle a(\phi,\psi)\rangle_{\{hkl\}}$ vs. $sin^2\psi$ plots, for which the splitting phenomenon was not observed (Fig. 6).

TABLE 1

Single crystal elastic constants used for calculation of diffraction elastic constants

	C_{11} (GPa)	C_{44} (GPa)	C_{12} (GPa)
ferrite	197	122	124
austenite	231	116.4	134.4
TiN	497	168	105

TABLE 2

Comparison of macrostresses and χ^2 values determined using different models for calculation of the diffraction elastic constants

Sample (X-ray radiation)	Grazing angle „α" (deg)	Pentration depth „t" (μm)	Stress component	Macrostresses (MPa), assuming $\sigma_{33} = 0$ (χ^2)		
				Voigt	Kröner	Reuss
ferritic steel -mechanical polishing	6	0.4	$\sigma_{11} = \sigma_{22}$	-1011 ± 30 (5.8)	-904 ± 27 (2.5)	-715 ± 21 (10.4)
	12	0.7	$\sigma_{11} = \sigma_{22}$	-851 ± 32 (9.9)	-770 ± 29 (4.9)	-577 ± 13 (22.7)
(Cu - radiation)	18	0.9	$\sigma_{11} = \sigma_{22}$	-609 ± 37 (12.7)	-586 ± 34 (7.0)	-415 ± 25 (11.3)
austenitic steel - grinding	6	1.7	σ_{11} σ_{22}	1361 ± 27 706 ± 19 (101.7)	1272 ± 19 604 ± 19 (28.7)	1007 ± 14 398 ± 14 (40.0)
(Fe - radiation)	12	3.0	σ_{11} σ_{22}	1225 ± 22 705 ± 22 (96.2)	1114 ± 18 577 ± 18 (36.4)	861 ± 14 358 ± 14 (30.5)
	18	4.0	σ_{11} σ_{22}	1152 ± 23 758 ± 23 (70.8)	1018 ± 19 576 ± 19 (20.0)	753 ± 14 334 ± 14 (17.2)
TiN coating on WC substrate	3	0.6	$\sigma_{11} = \sigma_{22}$	755 ± 7 (15.4)	753 ± 7 (13.2)	745 ± 7 (13.0)
(Co - radiation)	6	1.1	$\sigma_{11} = \sigma_{22}$	790 ± 7 (28.0)	736 ± 7 (27.0)	728 ± 7 (27.0)

Small differences between stresses determined by different models (Table 2) were found in the case of TiN coating for which the anisotropy of elastic constants was very low (Fig. 3). In this case, the measured and theoretical $\langle a(\phi,\psi)\rangle_{\{hkl\}}$ vs. $sin^2\,\psi$ curves exhibit approximately linear character for all models (Fig. 6). On the contrary, significant differences between stresses were obtained for different methods of diffraction elastic constants calculation in the case of steel samples (Table 2). The elastic anisotropy of crystallites was important for the ferritic and austenitic steels, as well (Fig.3). The $\langle a(\phi,\psi)\rangle_{\{hkl\}}$ vs. $sin^2\,\psi$ curves measured for the steel samples were not linear and the character of non-linearities was predicted by the K r ö n e r and R e u s s models (Figs 5 and 6). The quality of fitting was described by the χ^2 parameter defined as [20]:

$$\chi^2 = \frac{1}{K-L}\sum_{i=1}^{K}\frac{(\langle a(\phi,\psi)\rangle_i^m - \langle a(\phi,\psi)\rangle_i^t)^2}{\delta_i^2}, \tag{19}$$

where: K is the number of measured points, L is the number of fitting parameters in Eq. 4, $\langle a(\phi,\psi)\rangle_i^m$ is the experimental lattice parameter, $\langle a(\phi,\psi)\rangle_i^t$ is the theoretical value obtained from fitting procedure and δ_i is the standard deviation for the *i-th* measurement.

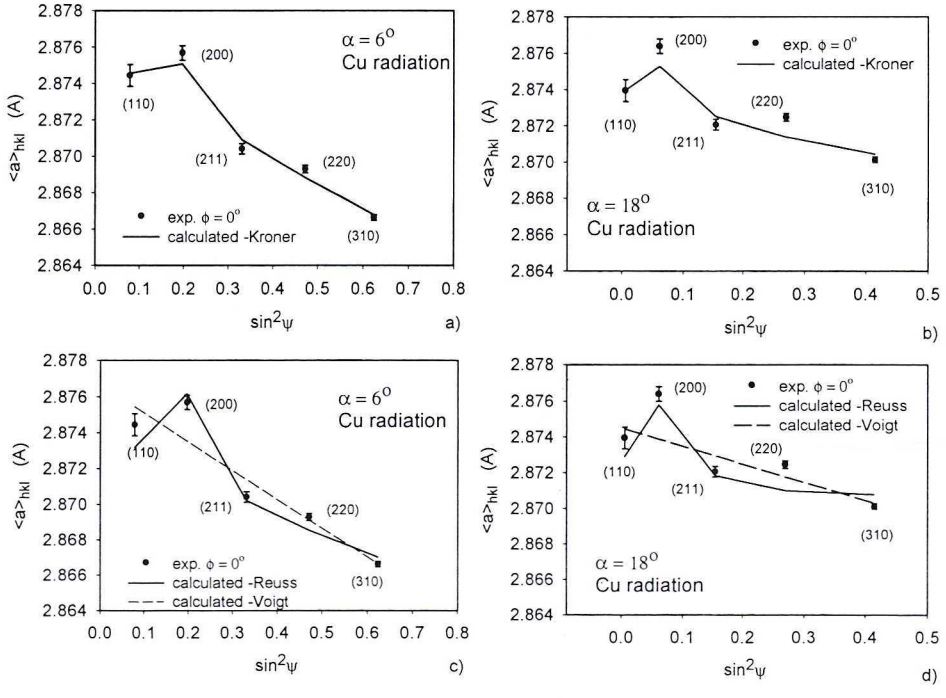

Fig. 5. The $\langle a(\phi,\psi)\rangle_{\{hkl\}}$ lattice parameters fitted to experimental points for grinded austenite. The same comparison as in Fig.4 is presented

Comparing the values of χ^2 and the $\langle a(\phi,\psi)\rangle_{\{hkl\}}$ vs. $sin^2\,\psi$ curves for different models, the best quality of fitting was found for the K r ö n e r approach (Table 2 and Figs 5 and 6).

Results obtained by the V o i g t model were very far from the experimental points due to linear character of the theoretical $\langle a(\phi,\psi)\rangle_{\{hkl\}}$ vs. $sin^2\psi$ curves (Figs. 5 and 6). On the contrary, in the case of the R e u s s model the non-linearities of theoretical curves were overestimated in comparison with the experimental points (Figs. 5 and 6). For a number of $\langle a(\phi,\psi)\rangle_{\{hkl\}}$ vs. $sin^2\psi$ curves a similar quality of fitting and significantly different stresses (for example austenitic sample - Table 2) were obtained using the R e u s s and K r ö n e r approaches.

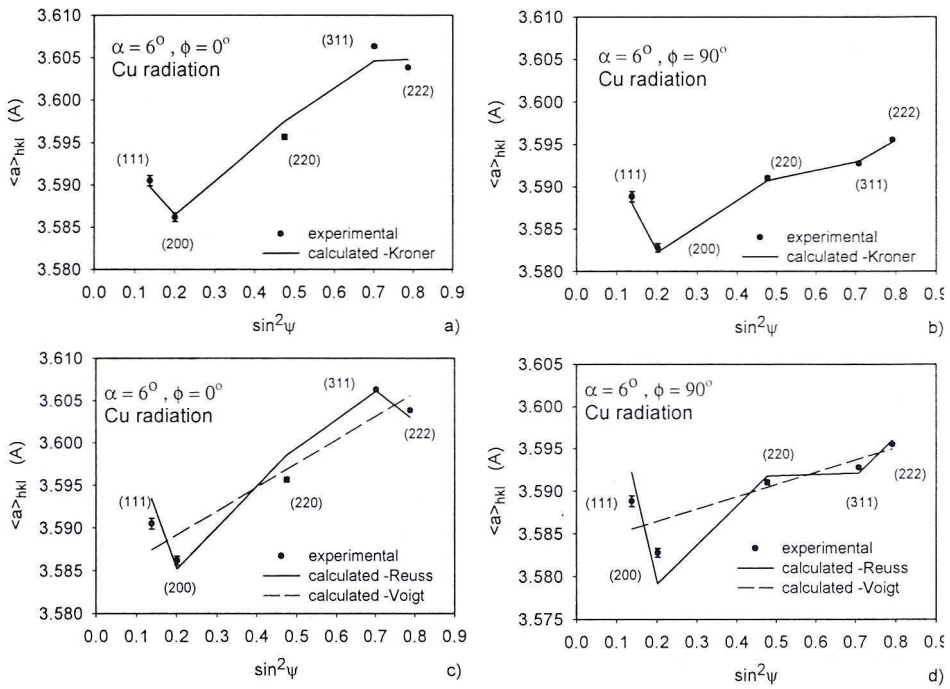

Fig. 6. The $\langle a(\phi,\psi)\rangle_{\{hkl\}}$ lattice parameters fitted to the experimental points for TiN coating deposited on WC substrate. The same comparison as in Figs. 4 and 5 is presented

As already mentioned, excellent predictions of non-linearity were obtained when the Kröner method was used for diffraction elastic constants predictions. This convergence proves that elastic anisotropy is correctly predicted by self consistent calculations, in which the interaction between grains is considered. The stress values obtained by the K r ö n e r method are always between the limits given by the V o i g t and R e u s s models (Table 2).

5. Conclusions

The $g\text{-}sin^2\psi$ geometry was used to measure residual stresses in a near surface volume of polycrystalline materials. The advantage of the $g\text{-}sin^2\psi$ method is that the penetration depth of the X-ray diffraction is constant during experiment and it can be easily changed by setting

various values of the incident angle α (Fig.2). The method can be used to find variation of the stresses below the sample surface.

The diffraction elastic constants calculated using the Kröner, Voigt and Reuss models were applied for interpretation of the experimental data obtained from the $g\text{-}sin^2\psi$ method. In the case of Kröner approach the elastic interaction between polycrystalline grains were calculated by the self-consistent scheme. For verification of different models, the effect of elastic anisotropy was studied comparing the experimental and theoretical non-linearities of the $<a(\phi,\psi)>_{\{hkl\}}$ vs. $sin^2\psi$ curves. A good agreement between measured and calculated results was obtained when the diffraction elastic constants were computed by the Kröner method. The values of residual stresses were obtained by fitting of the theoretical $<a(\phi,\psi)>_{\{hkl\}}$ vs. $sin^2\psi$ curves to the experimental points. The stresses determined using the Kröner approach were always between the limits obtained from the extreme models (i.e., the Voigt and Reuss methods).

Acknowledgements

This work has been partially supported the Polish Committee for Scientific Research (KBN) and by the Polish-French Integrated Program POLONIUM 2003 (Nr. 03270RD).

REFERENCES

[1] H. Wohlfahrt, R. Kopp, O. Vohringer, Shot Peening, Deutsche Gesellschaft fur Metallkunde, 1987.
[2] S.R. Brown, I.G. Turner, H. Reiter, J. Mater. Sci. Mater. Med. **5**, 756 (1994).
[3] D.S. Rickerby, A.M. Jones and B.A. Bellamy, Surface and Coat. Technology **37**, 111 (1989).
[4] I.C. Noyan, J.B. Cohen, Residual Streess: New York: Springer-Verlag, 1987.
[5] B.D. Cullity, Elements of X-ray Diffraction, 3rd ed. Massachussetts: Addison-Wesley, 1967
[6] K. Van Acker, L. De Bayser, J.P. Celis, P. Von Houtte. J. Appl. Cryst. **27**, 56 (1994).
[7] C. Quaeyhaegens, G. Knuyt. Surface and Coat. Technology **74/75**, 104 (1995).
[8] S.J. Skrzypek, Inżynieria Materiałowa **4**, 1035 (1998).
[9] S. J. Skrzypek, A. Baczmański, W. Ratuszek, E. Kusior, J. Appl. Cryst. **34**, 427 (2001).
[10] S.J. Skrzypek, A. Baczmański, Adv. X-Ray Diffraction **44**, 134 (2001)
[11] H.J. Bunge, Texture Analysis in Material Science: Mathematical Methods, Butterworths, London, 1982.
[12] H.J. Dolle, J. Appl. Cryst. **12**, 489 (1979).
[13] A. Baczmański, K. Wierzbanowski, W.G. Haije, R.B. Helmholdt, G. Ekambaranathan, B. Pathiraj, Cryst. Res. Technol. **28**, 229 (1993).
[14] W. Voigt, Lehrbuch der Kristallphysik, Leipzig, BG Teubner Verlag, 1928.
[15] A. Reuss, Z. Angew. Math. Mech. **9**, 49 (1929).
[16] E. Kröner, Acta Metall. Mater. **9**, 155 (1961).
[17] P. Lipiński, M. Berveiller, Int. J. of Plasticity **5**, 149 (1989).
[18] P. Lipiński, M. Berveiller, E. Reubrez, J. Morreale, Arch. Appl. Mech. **65**, 291 (1995).
[19] J.D. Eshelby. Proc. Roy. Soc. Lond. **A241**, 376 (1957).
[20] W.H. Press, B.P. Flannery, S.A. Teukolsky, W.T. Vetterling, Numerical Recipes, The Art of Scientific Computing: Cambridge University Press, 1989.

REVIEWED BY: JAN BONARSKI
Received: 20 March 2003.